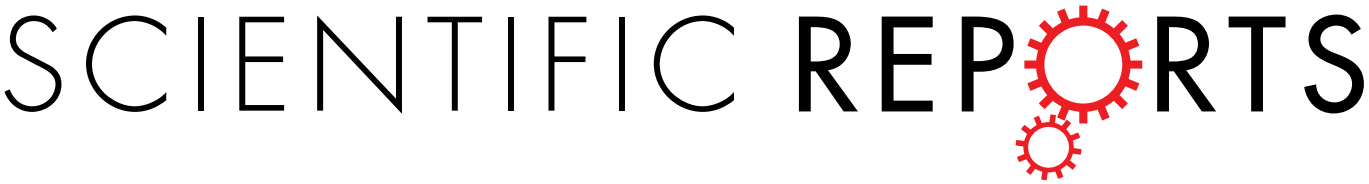

OPEN

Coexistence of superconductivity and charge-density wave in the quasi-one-dimensional material $HfTe_3$

Received: 28 November 2016
Accepted: 20 February 2017
Published: 24 March 2017

Saleem J. Denholme[1], Akinori Yukawa[1], Kohei Tsumura[1], Masanori Nagao[2], Ryuji Tamura[3], Satoshi Watauchi[2], Isao Tanaka[2], Hideaki Takayanagi[1] & Nobuaki Miyakawa[1]

We present the first experimental evidence for metallicity, superconductivity (SC) and the co-existence of charge density waves (CDW) in the quasi-one-dimensional material $HfTe_3$. The existence of such phenomena is a typical characteristic of the transition metal chalcogenides however, without the application of hydrostatic pressure/chemical doping, it is rare for a material to exhibit the co-existence of both states. Materials such as $HfTe_3$ can therefore provide us with a unique insight into the relationship between these multiple ordered states. By improving on the original synthesis conditions, we have successfully synthesised single phase $HfTe_3$ and confirmed the resultant structure by performing Rietveld refinement. Using low temperature resistivity measurements, we provide the first experimental evidence of SC at ~1.4 K as well as a resistive anomaly indicative of a CDW formation at ~82 K. By the application of hydrostatic-pressure, the resistivity anomaly shifts to higher temperature. The results show that $HfTe_3$ is a promising new material to help study the relationship between SC and CDW.

The coexistence of superconductivity (SC) and charge- and/or spin-density waves (CDW and/or SDW) is fundamental to our understanding behind the mechanism of high-T_c SC and is one of the most significant challenges in condensed matter physics[1]. CDWs favor low dimensionality[2] and materials such as the layered/chain-like transition metal di/trichalcogenides (MQ_2/Q_3) (where M = groups IV–VI transition metals and Q = sulfur, selenium and tellurium) have been collectively studied for such phenomena[3]. Examples include TaS_3[4] and NbS_3[5] which exhibit CDWs and $TaSe_3$ which becomes a SC below 2.1 K[6]. Studies of SC in the MQ_2/Q_3 family often support a competitive relationship between the SC and CDW states; SC can be induced/enhanced by the suppression of the CDW. This is typically achieved by the application of hydrostatic pressure such as in the case of $NbSe_2$[7] and $NbSe_3$[8] or by chemical doping for Na_xTaS_2[9] and Cu_xTiSe_2[10]. However, it is rare that the materials without chemical/physical modification exhibit the co-existence of both states. $ZrTe_3$ is a material which shows the coexistence of a CDW at ~63 K and filamentary SC at 2 K[11] as does $NbSe_2$[3]. In the case of $ZrTe_3$, by the application of pressure, intercalation of Cu[12] and Ni[13] or the substitution of Se at the Te site[14], the CDW can be suppressed and bulk SC induced at ~5 K[15]. The electronic structure of $ZrTe_3$ is unique amongst the MQ_3 family owing to the strong contribution of the Te-Te p_{σ^*} band at the vicinity of the Fermi level[16], therefore the inter-chain interactions affects the electronic structure as well as the physical properties. Similar cross-chain interactions are absent in other members of the MQ_3 family (when M = group IV transition metal and Q = S/Se)[17]. Of the MTe_3 materials, $HfTe_3$ is the only other material expected theoretically[18,19]. There are no known reports for $TiTe_3$ nor Nb/$TaTe_3$. However, by using the reaction conditions outlined by Brattås *et al.* we found that the successful synthesis of $HfTe_3$[18,19] was irreproducible. Therefore, although theoretical band structure calculations have predicted $HfTe_3$ to be metallic[16,20,21] there is currently no experimental confirmation. As far as the authors are aware, the available experimental data for $HfTe_3$ include the original structural characterization[18], and the determination of its basic magnetic properties (temperature-independent diamagnetism)[19]. In addition, it has been recently reported by scanning tunneling

[1]Tokyo University of Science, Department of Applied Physics, Tokyo, 125-8585, Japan. [2]University of Yamanashi, Centre for Crystal Science and Technology, Yamanashi, 400-8511, Japan. [3]Tokyo University of Science, Department of Materials Science and Technology, Tokyo, 125-8585, Japan. Correspondence and requests for materials should be addressed to S.J.D. (email: sdenholme@rs.tus.ac.jp) or N.M. (email: miyakawa@rs.tus.ac.jp)

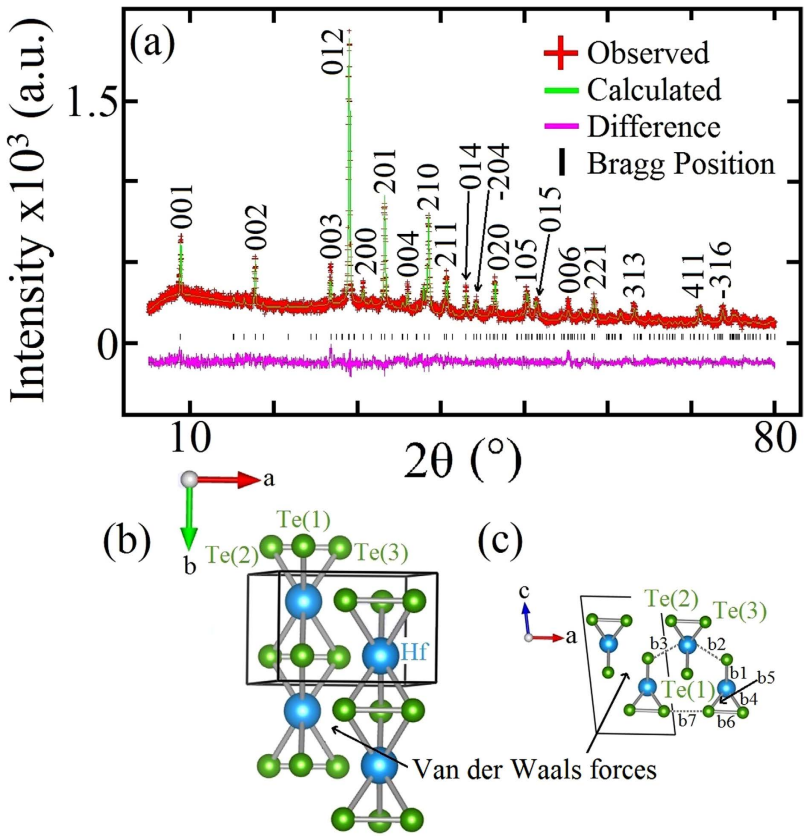

Figure 1. (**a**) Rietveld analysis of the PXRD results for $HfTe_3$. (**b**) Crystal structure of $HfTe_3$ revealing the anisotropic growth preferential along the *b*-axis. (**c**) Projection down the *b*-axis showing more clearly the separation of the chains, where the chains are weakly bonded by the Van der Waals forces. The positions of the three non-equivalent Te atoms are defined as Te(1), Te(2) and Te(3) and bond distances are indicated by b1-b7. The unit cell is indicated by the black lines.

spectroscopy that $Hf/HfTe_5/HfTe_3$ films exhibited a superconducting gap-like spectra[22]. $HfTe_3$ and $ZrTe_3$ are iso-structural materials whose features raise the possibility that $HfTe_3$ may also exhibit the coexistence of SC and CDW state. Therefore, it would be an important task to synthesize the high quality bulk compound, and to explore the aforementioned electrical phenomena.

By modifying the original synthesis conditions[18,19], polycrystalline $HfTe_3$ samples have been successfully synthesized. The crystal structure has been analyzed using Rietveld refinement and the first experimental evidence of metallicity in this material is reported. The resistivity data exhibits an anomaly suggestive of a CDW formation at ~82 K and subsequently zero resistivity below 2 K. By the application of hydrostatic pressure, the resistivity anomaly shifts to higher temperature. In addition, we note that $HfTe_3$ is highly air-sensitive, where the behaviour of ρ-T characteristics changes from metallic to insulating upon exposure in air (See Supplementary information).

Results and Discussion

Key requirements to synthesise single phase $HfTe_3$. Suitable reaction conditions to produce single phase $HfTe_3$ crucially depend on the maximum reaction temperature[19]. During this investigation it has been found that a slow cooling rate is also a key requirement. In brief, the favoured phase was $HfTe_2$ at a higher temperature range ($\geq$530 °C) and $HfTe_5$ at lower temperature regions ($\leq$470 °C). As reported by Brattås *et al.*, we confirmed that the sintering condition of c.a. 500 °C indeed favours the growth of the $HfTe_3$ phase[18]. However, when rapid cooling from 500 °C (*e.g.* quenching in water) was applied[19] the majority phase became $HfTe_2$ together with unreacted tellurium. On the other hand, when slow cooling was performed (approx. −0.25 °C/h) until 470 °C after which the ampoules were cooled to room temperature at a rate of approx. −5 °C/h, then single phase $HfTe_3$ could reproducibly be synthesised. The results suggest that $HfTe_3$ primarily forms by reaction with the tellurium vapour upon cooling. If the reaction vessel is quenched, the solidification of the tellurium prevents its uptake and $HfTe_2$ becomes the preferred phase. Namely, it is found that $HfTe_3$ is the least thermodynamically stable phase within the Te-rich Hf alloys and as a result in order to inhibit the formation of trace amounts of $HfTe_2/HfTe_5$, it is necessary to control precisely both the sintering temperature and the cooling rate.

Crystallographic analysis. Figure 1(a) shows the powder X-ray diffraction (PXRD) result for $HfTe_3$ together with the result of the Rietveld refinement using $ZrSe_3$ as a reference model[23], where the result was consistent with the monoclinic crystal symmetry (space group $P2_1/m$). Figure 1(b) represents the crystal structure

Crystal system	Monoclinic	No. Observations	7500,
Space group	$P2_1/m$ (No. 11)	No. parameters	31
a (Å)	5.8797 (9)	R_{wp}	0.0847
b (Å)	3.8999 (9)	R_p	0.066
c (Å)	10.0627 (3)	Goodness of fit, χ^2	1.544
β (°)	98.38 (8)	Temperature (K)	295 K
V (Å^3)	228.28 (2)		
Z	2		
Hf; 2*e* (x, 1/4, z)		Te(1); 2*e* (x, 1/4, z)	
x	0.2590 (7)	x	0.7339 (7)
z	0.6881 (2)	z	0.5674 (3)
100 x U_{iso} (Å^2)*	0.484	100 x U_{iso} (Å^2)	0.484
Occ	1	Occ	1
Te(2); 2*e* (x, 1/4, z)		Te(3); 2*e* (x, 1/4, z)	
x	0.4173 (7)	x	0.9058 (6)
z	0.1625 (9)	z	0.1638 (3)
100 x U_{iso} (Å^2)*	0.484	100 x U_{iso} (Å^2)*	0.484
Occ	1	Occ	1
Selected bond lengths (Hf-Te) (Å)		Selected bond lengths (Te-Te) (Å)	
Hf - Te(1) x2 (b1)†	3.074 (6)	Te(2) - Te(3) x1 (b6)†	2.870 (13)
Hf - Te(1) x1 (b2)†	3.106 (8)	Te(2) - Te(3) x1 (b7)†	3.010 (13)
Hf - Te(1) x1 (b3)†	3.106 (6)		
Hf - Te(2) x2 (b4)†	3.062 (7)		
Hf - Te(3) x2 (b5)†	2.843 (6)		

Table 1. Crystallographic data for $HfTe_3$. *Isotropic displacement factors were constrained during refinement. †Refer to Fig. 1(c).

of $HfTe_3$ which is the pseudo-one-dimensional (1D) structure. As seen in Fig. 1(b), MQ_6 trigonal prismatic units propagate along the *b*-axis resulting in chain-like anisotropic crystal growth. By projection down the *b*-axis it can be clearly seen how the chains are bonded together by Van der Waals forces (see Fig. 1(c)). Reasonable values of $R_{wp} = 8.47\%$, $R_p = 6.60\%$ and $\chi^2 = 1.544$ were obtained. Refined lattice parameters of $HfTe_3$, $a = 5.8797(9)$ Å, $b = 3.8999(9)$ Å, $c = 10.0627(3)$ Å agreed with the previously reported values[19]. On the other hand, the angle $\beta = 98.38(8)°$ showed a slight expansion from the originally reported angle of $\beta = 97.98°$[18]. The refinement results are summarized in Table 1. It was confirmed from X-ray fluorescence (XRF) results that the composition ratio of our $HfTe_3$ was Hf:Te = 26:74 (at%).

Coexistence of SC and CDW. Resistivity of non-air-exposed $HfTe_3$ reproducibly exhibited metallic behaviour in the temperature range between 0.3 and 300 K as shown in Fig. 2(a). The residual resistivity ratio (RRR) defined as $\rho(275\,K)/\rho(4\,K)$ is ~2.4, which is lower than that of single crystal $ZrTe_3$[11] but is larger than that of polycrystalline-$ZrTe_3$[24], in which the lower RRR value is thought to arise from strong grain boundary effects. Therefore the influence of grain boundaries is likely to play a role in the reduction of RRR. The inset of Fig. 2(a) shows the temperature derivative of the resistivity $d\rho/dT$ and reveals a resistivity anomaly at 82 K assumed to be indicative of a CDW formation, where the CDW formation temperature T_{CDW} is defined as the temperature at which $d\rho/dT$ exhibits a minimum. At T_{CDW} the CDW gap is developed and the resistance anomaly appears owing to a reduction in the density of states at E_F due to the CDW formation. Below 2 K, the resistivity showed a sharp drop exhibiting a SC transition at 1.8 K (T_c^{onset}) and reached zero (T_c^{zero}) at 1.45 K as can be clearly seen in Fig. 2(b). By increasing the applied current, a broadening of the SC transition was observed and it was accompanied by a downward shift in T_c^{onset} and T_c^{zero}, whereas the normal state resistivity remains unchanged. The result suggests a weakening in the SC state as well as a decoupling of the Josephson junctions between individual SC grains of the polycrystalline material. *I–V* characteristics measured at $T > T_c$ and $T < T_c$ revealed ohmic and non-ohmic behaviour, respectively. N.B. In the present study, we observe that $HfTe_3$ shows a rapid weakening of its metallic state within minutes of exposure in air (see Supplementary Fig. S1). This is likely the result of an insulating layer (such as tellurium oxides) forming around the individual grains of the polycrystalline material. The results emphasize that if one is to observe the intrinsic properties of $HfTe_3$ any measurements must be conducted in the absence of air.

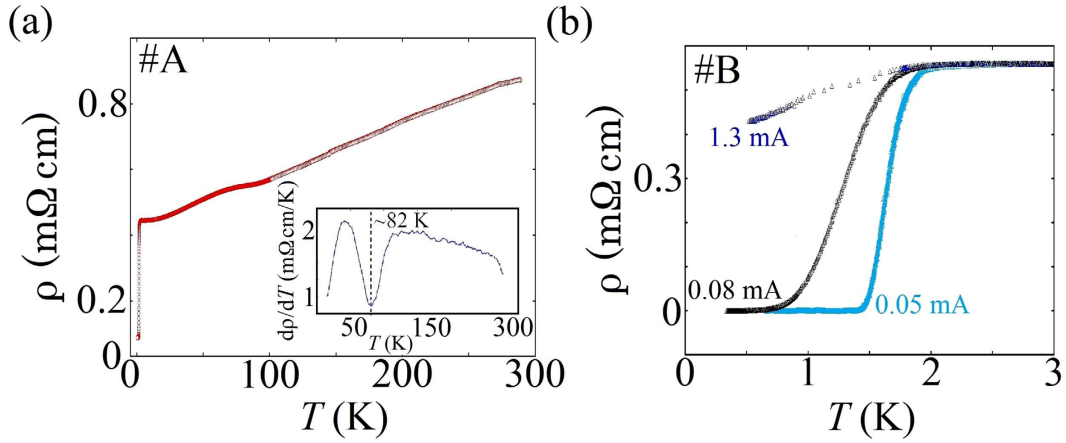

Figure 2. (**a**) Temperature dependence of the resistivity for $HfTe_3$. Data show a hump-like feature at ~80 K together with and SC-like transition at 1.8 K. Inset shows that the resistivity anomaly occurs at approximately 82 K (sample #A). (**b**) Current dependency of the resistivity of $HfTe_3$ below 3 K. T_c^{onset} is approximately 1.8 K and T_c^{zero} is reached c.a. 1.4 K for a current of 0.05 mA. By an increase in current, both the T_c^{onset} and T_c^{zero} show a shift to lower temperatures (sample #B).

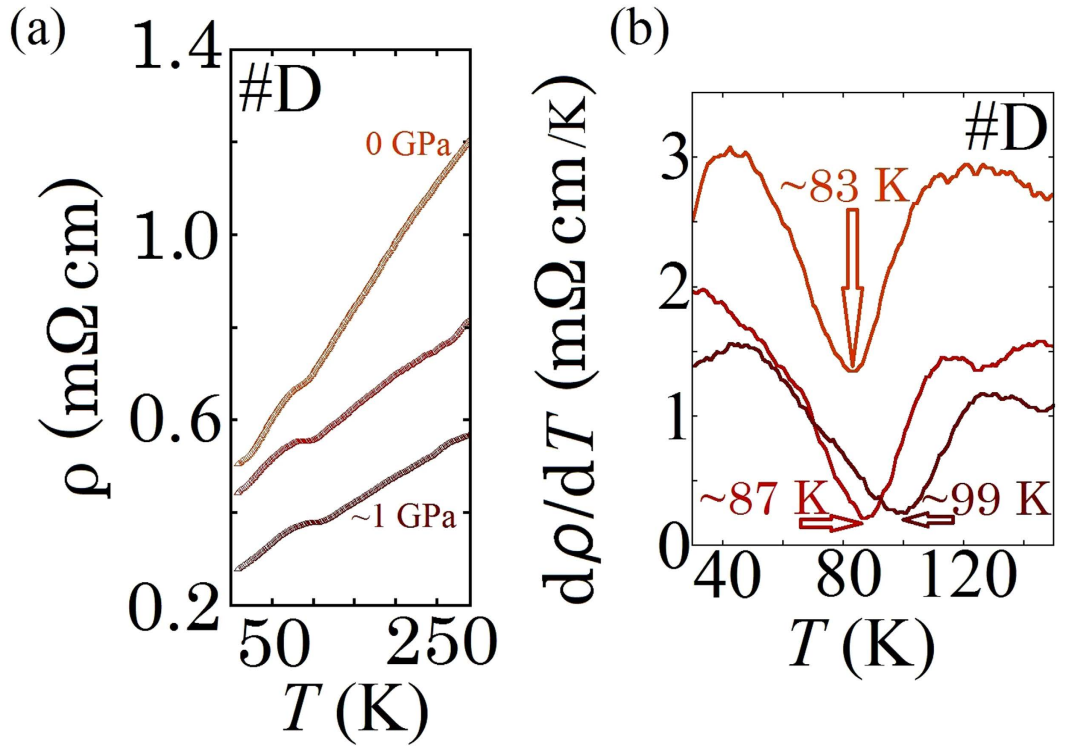

Figure 3. (**a**) Pressure dependence of resistivity at the range of $P = 0$–1 GPa. (**b**) $d\rho/dT$ in the range of 30–150 K as a function of pressure. The minimum of the dip structure shows a shift to higher T with increasing P. Color coding between (**a** and **b**) are matched to indicate the same pressure values (sample #D).

Behaviour under high-pressure. By the application of hydrostatic pressure (P), the resistivity anomaly gradually shifted to higher temperatures up to ~99 K for P approaching 1 GPa as shown in Fig. 3. Similar behaviour has been reported for $ZrTe_3$ where in the case of an application of $P \leq 2$ GPa the T_{CDW} was increased and the SC suppressed. At $P \geq 5$ GPa the CDW was fully quenched and gave way to reemergent SC, where T_c increased to ~4.5 K when P~11 GPa[15]. In addition, in the case of $HfTe_5$, SC appeared by applying P~5 GPa and a maximum T_c of 4.8 K was attained by applying at P~20 GPa[25]. This suggests the possibility that $HfTe_3$ is likely to follow the same pattern as other members of the group IV-MTe_x alloys. Namely by further application in pressure, it is expected that the T_{CDW} will eventually be suppressed and T_c will be enhanced.

Electronic structure. Studies regarding the electronic structure of $HfTe_3$ are limited, but the issue is briefly reported by Felser *et al.* who determined an electronic structure similar to that of $ZrTe_3$, *i.e.* a metallic state resulting from a large contribution of the Te *p*-bands at the Fermi level[16]. These characteristics are supported by later density of states (DOS) calculations[20,21]. $ZrTe_3$ exhibits a multi-component Fermi surface with contributions from the Te forming quasi 1D electronic sheets at the boundary of the Brillion zone and from the Zr a 3D-hole character sheet around the Γ point. The resultant nesting characteristics at the Fermi surface have been determined to be responsible for the CDW formation in $ZrTe_3$[16,26–28]. If one considers the iso-structural/electronic relationship between $HfTe_3$ and $ZrTe_3$, it is likely that similar interchain interactions between neighbouring Te(2) and Te(3) atoms (see Fig. 1(c)) play a dominant role in the metallicity of $HfTe_3$[16] which in turn would give rise to the similar Fermi surface with nesting features reported for $ZrTe_3$. However, it cannot be categorically asserted that the observed resistivity anomaly is due to a CDW formation from our results only. As in the case of $ZrTe_3$, it would be necessary to confirm any coincidental low-temperature lattice distortions[29] as well as to observe the features of the Fermi surface around the temperature of the anomaly[26]. However the similarities between $HfTe_3$ and $ZrTe_3$ in the electronic structure as well as the results of the temperature/pressure dependence of ρ are strong indication that the observed resistivity anomaly for $HfTe_3$ is indeed the result of a CDW formation.

Conclusion

In summary, we have established a reproducible synthesis method for high-quality polycrystalline $HfTe_3$ and showed that it is an acutely air-sensitive material. By using high-quality $HfTe_3$ we found that the quasi-1D $HfTe_3$ is a novel SC with $T_c \sim 1.4$ K, and the SC state coexists with the CDW state which appears at $T_{CDW} \sim 82$ K. Furthermore, we provided the first accurate crystallographic data by Rietveld refinement of the PXRD of $HfTe_3$.

Methods

Single-phase polycrystalline $HfTe_3$ samples have been prepared using standard chemical vapour transport techniques. Ground mixtures of a 1:3 molar ratio of powdered Hf and Te were sealed in silica ampoules under a vacuum of c.a. 3 mTorr using a rotary pump. The ampoules were heated in a box furnace using the reaction procedure described in the results and discussion. To prevent exposure to air, all sample preparation was conducted in an argon filled glovebox.

PXRD was carried out using a Rigaku Smartlab diffractometer in flat plate geometry with a Cu K_α radiation ($\lambda = 1.54056$ Å). Diffraction data were typically collected for $5° \leq 2\theta \leq 80°$ with a 0.01° step size with scan times of 3 hours. Rietveld refinement was performed using the GSAS software package via the EXPGUI interface[30,31]. XRF analysis was performed using a JEOL JSX 1000 S ElementEye.

Resistivity measurements were performed on cold-pressed pellets using a standard four-terminal setup. Measurements for sample #A were performed between 0.3 and 300 K using an Oxford Instruments 3He cryostat, data were collected by an AC method using a low-noise amplifier and two lock-in amplifiers. Measurements for sample #B were performed by a DC method between 0.3 K and 15 K using a Quantum Design PPMS equipped with an adiabatic demagnetization refrigerator. The resistivity for Samples #C and #D were also measured by a DC method between 2 and 300 K using a closed cycle helium refrigerator. High-pressure resistivity measurements (up to 1 GPa) were performed using a BeCu/NiCrAl clamped piston-cylinder cell using Daphne 7373 as the fluid pressure transmitting medium with Pb employed as a manometer.

References

1. Gabovich, A. M., Voitenko, A. I. & Ausloos, M. Charge- and spin-density waves in existing superconductors: competition between cooper pairing and peirels or excitonic instabilities. *Phys. Rep*. **367,** 583–709 (2002).
2. Grüner, G. The dynamics of charge-density waves. *Rev. Mod. Phys*. **60,** 1129–1178 (1988).
3. Wilson, J. A., Di Salvo, F. J. & Mahajan, S. Charge-density waves and superlattices in the metallic layered transition metal dichalcogenides. *Adv. Phys*. **24,** 117–201 (1975).
4. Ido, M., Tsutsumi, K., Sambongi, T. & Mori, N. Pressure dependence of the metal-semiconductor transition in TaS_3. *Solid State Comm*. **29,** 399–402 (1979).
5. Wang, Z. *et al.* Charge-density-wave transport above room temperature in a polytype of NbS_3. *Phys. Rev. B*. **40,** 11589 (1989).
6. Yamamoto, M. Superconducting properties of $TaSe_3$. *J. Phys. Soc. Jpn*. **45,** 431–438 (1978).
7. Suderow, H., Tissen, V. G., Brison, J. P., Martínez, J. C. & Viera, S. Pressure induced effects on the fermi surface of superconducting 2H-$NbSe_2$. *Phys. Rev. Lett.* **95,** 117006 (2005).
8. Núñez Reguerio, M., Mignot, J. M. & Castello, D. Superconductivity at high pressure in $NbSe_3$. *Europhys. Lett*. **18,** 53–57 (1992).
9. Fang, L. *et al.* Fabrication and superconductivity of Na_xTaS_2 crystals. *Phys. Rev. B*. **72,** 014534 (2005).
10. Morosan, E. *et al.* Superconductivity in Cu_xTiSe_2. *Nature Phys*. **2,** 544–550 (2006).
11. Takahashi, S., Sambongi, T., Brill, J. W. & Roark, W. Transport and elastic anomalies in $ZrTe_3$. *Solid State Comm*. **49,** 1031–1033 (1984).
12. Zhu, X., Lei, H. & Petrovic, C. Coexistence of bulk superconductivity and charge density wave in Cu_xZrTe_3. *Phys. Rev. Lett.* **106,** 246404 (2011).
13. Lei, H., Zhu, X. & Petrovic, C. Raising T_c in charge density wave superconductor $ZrTe_3$ by Ni intercalation. *EPL*. **95,** 17011 (2011).
14. Zhu, X. *et al.* Superconductivity and charge density wave in $ZrTe_{3-x}Se_x$. *Sci. Rep*. **6,** 26974 (2016).
15. Yomo, R., Yamaya, K., Abliz, N., Hedo, M. & Uwatoko, Y. Pressure effect on competition between charge density wave and superconductivity in $ZrTe_3$: appearance of pressure-induced reentrant superconductivity. *Phys. Rev. B*. **71,** 132508 (2005).
16. Felser, C., Finckh, E. W., Kleinke, F., Rocker, F. & Tremel, W. Electronic properties of $ZrTe_3$. *J. Mater. Chem*. **8,** 1787–1798 (1998).
17. Srivastava, S. K. & Avasthi, B. N. Preparation, structure and properties of transition metal trichalcogenides. *J. Mater. Sci.* **27,** 3693–3705 (1992).
18. Brattås, L. & Kjekshus, A. The non-metal rich region of the Hf-Te system. *Acta Chem. Scand.* **25,** 2783–2784 (1971).
19. Brattås, L. & Kjekshus, A. On the properties of compounds with the $ZrTe_3$ type structure. *Acta Chem. Scand.* **26,** 3441–3449 (1972).
20. Abdulsalam, M. & Joubert, D. P. Structural and electronic properties of MX_3 (M = Ti, Zr and Hf; =S, Se, Te) from first principles calculations. *Eur. Phys. J. B*. **88,** 177 (2015).
21. Li, M., Dai, J. & Cheng-Zeng, X. Tuning the electronic properties of transition-metal trichalcogenides *via* tensile strain. *Nanoscale* **7,** 15385–15391 (2015).

22. Wang, Y. *et al.* Spontaneous formation of a superconductor-topological insulator-normal metal layered heterostructure. *Adv. Mater.* **28,** 5013–5017 (2016).
23. Furuseth, S., Brattås, L. & Kjekshus, A. On the crystal structures of TiS_3, ZrS_3, $ZrSe_3$, $ZrTe_3$, HfS_3 and $HfSe_3$. *Acta Chem. Scand.* **29,** 623–631 (1975).
24. Yadav, C. S. & Paulose, P. L. Superconductivity at 5.2 K in $ZrTe_3$ polycrystals and the effect of Cu and Ag intercalation. *J. Phys.: Condens. Matter*. **24,** 235702 (2012).
25. Qi, Y. *et al.* Pressure-driven superconductivity in the transition-metal pentatelluride $HfTe_5$. *Phys. Rev. B*. **94,** 054517 (2016).
26. Kubo, Y. *et al.* Electron momentum density in the low dimensional layered system $ZrTe_3$. *J. Phys. Soc. Jpn.* **76,** 064711 (2007).
27. Stöwe, K. & Wagner, F. R. Crystal structure and calculated electronic band structure of $ZrTe_3$. *J. Solid State Chem.* **138,** 160–168 (1998).
28. Hoesch, M. *et al.* Splitting in the fermi surface of $ZrTe_3$: a surface charge density wave system. *Phys. Rev. B.* **80,** 075423 (2009).
29. Eaglesham, D. J., Steeds, J. W. & Wilson, J. A. Electron microscope study of superlattices in $ZrTe_3$. *J. Phys. C: Solid State Phys*. **17,** L697–L698 (1984).
30. Larson, A. C. & von Dreele, R. B. The General Structure Analysis system. *Los Alamos National Laboratories, Los Alamos, NM* (2000).
31. Toby, B. H. EXPGUI, a graphical user interface for GSAS. *J. Appl. Crystallogr*. **34,** 210–213 (2001).

Acknowledgements

The authors would like to thank Akikuni Tomonaga, Keita Miyake and Kensuke Yoshinaga, for their assistance in completing the sample analysis.

Author Contributions

S.J.D. and N.M. designed, performed the experiments and analysed the experimental data and wrote the manuscript. A.Y. helped with the sample synthesis. K.T., M.N., S.W., I.T. and H.T. helped collect the low temperature resistivity data at $T < 2$ K. R.T. helped collect the XRF data.

Additional Information

Supplementary information accompanies this paper at http://www.nature.com/srep

Competing Interests: The authors declare no competing financial interests.

How to cite this article: Denholme, S. J. *et al.* Coexistence of superconductivity and charge-density wave in the quasi-one-dimensional material $HfTe_3$. *Sci. Rep.* **7**, 45217; doi: 10.1038/srep45217 (2017).

Publisher's note: Springer Nature remains neutral with regard to jurisdictional claims in published maps and institutional affiliations.